ResearchGate

See discussions, stats, and author profiles for this publication at: https://www.researchgate.net/publication/49810872

Spectrochemical Series and the Dependence of Racah and 10Dq Parameters on the Metal−Ligand Distance: Microscopic Origin

ARTICLE *in* THE JOURNAL OF PHYSICAL CHEMISTRY A · FEBRUARY 2011

Impact Factor: 2.69 · DOI: 10.1021/jp110586e · Source: PubMed

CITATIONS
24

READS
186

6 AUTHORS, INCLUDING:

Miguel Moreno
Universidad de Cantabria
224 PUBLICATIONS **2,718** CITATIONS

SEE PROFILE

Available from: Miguel Moreno
Retrieved on: 26 January 2016

THE JOURNAL OF PHYSICAL CHEMISTRY A

ARTICLE

pubs.acs.org/JPCA

Spectrochemical Series and the Dependence of Racah and 10*Dq* Parameters on the Metal−Ligand Distance: Microscopic Origin

A. Trueba,[†] P. Garcia-Fernandez,[†] J. M. García-Lastra,[‡] J. A. Aramburu,[*,†] M. T. Barriuso,[§] and M. Moreno[†]

[†]Departamento de Ciencias de la Tierra y Física de la Materia Condensada, Universidad de Cantabria, Avenida de los Castros s/n, 39005 Santander, Spain

[‡]Center for Atomic-Scale Materials Design, Department of Physics, Technical University of Denmark, DK-2800 Kongens Lyngby, Denmark

[§]Departamento de Física Moderna, Universidad de Cantabria, Avenida de los Castros s/n, 39005 Santander, Spain

ABSTRACT: The origin of the spectrochemical series and the different dependence of crystal-field splitting (10*Dq*) and Racah parameters on the metal−ligand distance, *R*, is explored through ab initio calculations on Cr^{3+}-doped K_2NaScF_6, Cs_2NaYCl_6, Cs_2NaYBr_6, and Cs_2NaYI_6 lattices. For this purpose both periodic and cluster calculations have been performed. An analysis of ab initio results proves that 10*Dq* values mostly come from the small admixture of deep n_Ls ligand orbitals present in the antibonding $e_g(\sim x^2-y^2,3z^2-r^2)$ level and not from the dominant covalency with valence n_Lp ligand orbitals, which is actually responsible for the reduction of Racah parameters. This study thus reveals the microscopic origin of the stronger dependence upon *R* of 10*Dq* when compared to that observed for Racah parameters, thus explaining why electronic transitions which are 10*Dq*-independent give rise to sharp optical bands. As a salient feature, while the covalency with n_Lp levels increases significantly on passing from CrF_6^{3-} to CrI_6^{3-}, the n_Ls admixture in e_g is found to be practically unmodified. This fact helps to understand the progressive decrease of 10*Dq* through the series of CrF_6^{3-}, $CrCl_6^{3-}$, $CrBr_6^{3-}$, and CrI_6^{3-} complexes embedded in the corresponding host lattices when compared at the corresponding equilibrium distance at zero pressure. The growing importance of the n_Ls admixture is well-depicted using deformation density diagrams on passing from the ground state $^4A_2(t_{2g}^3)$ to the $^4T_2(t_{2g}^2e_g)$ excited state depicted at several *R* values.

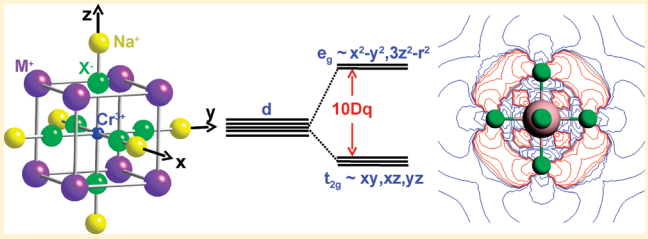

1. INTRODUCTION

A widespread interest on transition metal (TM) complexes formed through n_Md cations (n_M = 3−5) exists in physics, chemistry, and biology due to their particular properties. Indeed TM complexes are involved in molecular magnets and centers with giant magnetic anisotropy,[1−4] active centers of proteins,[5] catalysts,[6] molecular electronics,[7] pigments,[8−10] electroluminescent devices,[11] gemstones,[12−14] high-pressure manometers,[15,16] solid-state lasers,[17,18] and systems with ferroelectric distortions.[19,20] A general characteristic, common to all of these systems, is that the highest occupied molecular orbital (HOMO) level in the complex has an antibonding character arising from a n_Md level of free TM cation. Nevertheless, a partial splitting of mainly n_Md levels emerges even under octahedral (O_h) symmetry,[21] giving rise to the antibonding $e_g(\sim x^2-y^2,3z^2-r^2)$ and t_{2g} $(\sim xy,xz,yz)$ levels whose energy difference is called 10*Dq*. This quantity plays a key role for understanding the properties displayed by TM complexes. For instance, the nature and spin, *S*, of the ground-state and the associated magnetic properties for n_Md^m octahedral complexes with $3 < m < 8$ strongly depend[22,23] on the actual value of 10*Dq*. Furthermore, the transition from a broad band emission to a sharp one in the case of octahedral complexes of V^{2+}, Cr^{3+}, or Mn^{4+} impurities is favored[12,21,24,25] by an increase of 10*Dq*. In this case the first excited state is $^2E(t_{2g}^3)$, that is, 10*Dq*-independent, while in low crystal field cases it is $^4T(t_{2g}^2e_g)$. Along this line $t_{2g}^re_g^s \rightarrow t_{2g}^{r-1}e_g^{s+1}$ transitions in octahedral complexes induce an increase[26,27] of the metal−ligand distance, *R*, leading to a softening of stretching frequencies.[28−30] This phenomenon partially reflects the dependence of 10*Dq* upon *R*, which is also behind the Stokes shift, the Huang−Rhys factor with the symmetric mode, and the bandwidth of optical bands involving a $t_{2g} \rightarrow e_g$ electronic transition.[26,27,31−37] Optical data *for a given* complex taken at different *R* values reveal that 10*Dq* depends on R^{-n}, where *n* is usually found to lie close to 5.[31,38−41]

The difference between antibonding $e_g(x^2-y^2,3z^2-r^2)$ and $t_{2g}(xy,xz,yz)$ levels has also been pointed out[42] to be relevant for understanding why the $KNiF_3$ perovskite displays a perfect cubic symmetry while in $KMnF_3$ there is tilting of the MnF_6^{4-} octahedral at low temperature. Indeed it has recently been proved[42] that in KMF_3 compounds (M = $3d^m$ cation) tilting is suppressed by filling the t_{2g} shell.

Although both the 10*Dq* value for a given TM complex and its *R* dependence are currently well-reproduced by ab initio

Received: November 5, 2010
Revised: December 22, 2010
Published: February 4, 2011

ACS Publications © 2011 American Chemical Society

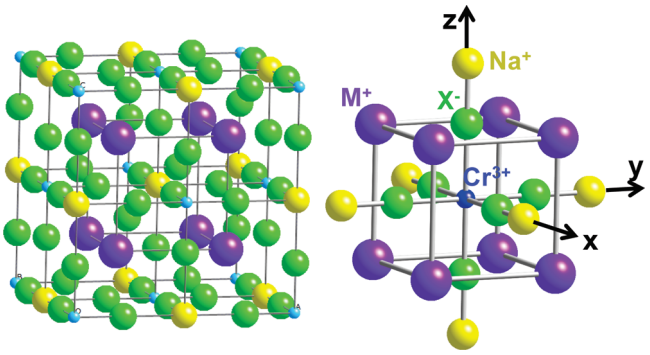

Figure 1. Periodic cell (left) and 21 ion cluster (right) employed for the density functional theory calculations of Cr^{3+}-doped M_2NaScX_6 and M_2NaYX_6 (X = F, Cl, Br, I; M = K, Cs) elpasolite lattices.

calculations,[27,43−46] there are still open questions concerning the actual *microscopic origin* of some relevant experimental facts involving the $10Dq$ parameter. One of such issues corresponds to the so-called spectrochemical series,[47] where a reduction of only about 20% in the $10Dq$ value of an octahedral MF_6^{q-} complex is observed when the F^- ligand is replaced by Br^-. This result cannot be simply understood on the basis of the equilibrium metal−ligand distance, R_e, which is approximately 30% higher in MBr_6^{q-} than in MF_6^{q-}. Indeed if $10Dq$ only depends on R^{-n} ($n = 5$), the $10Dq$ value for MF_6^{q-} should be about *four times* that for MBr_6^{q-}.

Another key point which needs to be understood concerns the much higher sensitivity of the $10Dq$ value of a given complex to variations of the metal−ligand distance when compared to that of the Racah parameters and also the covalency with valence n_Lp orbitals of ligands.[39,40,43,46,48,49] It should be noted that in an antibonding $e_g(x^2-y^2,3z^2-r^2)$ orbital of an octahedral MX_6^{q-} complex (X = halide) the n_Md levels are mixed *mainly* with n_Lp orbitals of ligands as the n_Ls orbitals lie below the n_Lp ones between 23 and 15 eV for free F^- and Br^-, respectively.[50] For this reason the n_Ls admixture has a *residual* character, far from typical sp^n ($n = 1-3$) hybridization schemes which are valid for atoms where n_Lp and n_Ls orbitals have much closer energies.[51] Available data of electron paramagnetic resonance (EPR) and theoretical calculations both indicate[46,49,52,53] that the amount of p_σ admixture in the $e_g(x^2-y^2,3z^2-r^2)$ orbital is nearly independent of R. In spite of the admixture of n_Ls ligand wave functions in the antibonding $e_g(x^2-y^2,3z^2-r^2)$ orbital being much smaller than that associated with the n_Lp covalency, semiempirical calculations have suggested that this mixing could play an important role for understanding the $10Dq$ value and its strong R dependence.[54]

Bearing in mind these facts, this work is aimed at gaining a better insight into the microscopic origin of the spectrochemical series and the different dependence of Racah parameters and $10Dq$ upon R. For properly achieving this goal ab initio calculations on large clusters simulating CrX_6^{3-} complexes (X = F, Cl, Br, I) embedded in cubic elpasolite A_2NaMX_6 ($A = K^+$, Cs^+; $M = Sc^{3+}$, Y^{3+}; $X = F^-$, Cl^-, Br^-, I^-) lattices[55] (Figure 1) have first been carried out. After obtaining the equilibrium distance at zero pressure, in a first step we have explored in detail the R dependence of Racah and $10Dq$ parameters and also that of n_Lp and n_Ls admixtures in the $e_g(x^2-y^2,3z^2-r^2)$. Aside from verifying that the main trends of experimental results are reasonably reproduced by ab initio calculations, particular attention is paid to unravel its actual microscopic origin. For achieving this goal we use a *model* where $10Dq$ is written in an approximate way as a sum of several contributions whose values are derived from the results provided by ab initio calculations. In that analysis special attention is addressed to the contribution coming from the calculated admixture with deep n_Ls orbitals, termed $10Dq_s$. Because the energy difference between the antibonding $e_g(x^2-y^2,3z^2-r^2)$ level and the n_Ls levels is in all cases larger than 18 eV, the $10Dq_s$ contribution is derived using a simple second-order approximation.[56]

The last part of the present study on CrX_6^{3-} complexes deals with the isotropic outward force on ligands[57] along the a_{1g} breathing mode, which appears as a result of the transition from the $^4A_2(t_{2g}^3)$ ground state to the first excited state $^4T_2(t_{2g}^2e_g)$ whose energy is just $10Dq$. By virtue of the Hellmann−Feynman theorem the quantity $d(10Dq)/dR$ is shown to be strongly connected with the *difference* of electronic density, $\Delta\rho_{GE}$, between excited state and ground state which is derived from the ab initio calculations. In this work, particular attention is addressed to the form of $\Delta\rho_{GE}$ in the neighborhood of ligand nuclei as far as the metal−ligand distance, R, is modified. This study provides us with additional information on the change of n_Ls−n_Lp hybridization in the $e_g(x^2-y^2,3z^2-r^2)$ orbitals upon variations of R.

The present work is arranged as follows. In section 2 is explained how a reasonable value of the $10Dq_s$ contribution is obtained from ab initio calculations. In addition, an estimation of the contribution to $10Dq$ coming from the n_Md−n_Lp hybridization in $e_g(x^2-y^2,3z^2-r^2)$ and $t_{2g}(xy,xz,yz)$ orbitals is also given in that section following a procedure similar to that first put forward by Anderson.[58] The computational tools employed in the present work are shortly described in section 3. In section 4 are exposed the main results given by ab initio calculations on the four explored systems together with the analysis carried out in this work by means of the model. Finally some last remarks are given in section 5.

2. THEORETICAL BASIS FOR THE ANALYSIS

An octahedral MX_6^{q-} complex involves a central cation, M, and halide ligands, X (X = F, Cl, Br, I), which, respectively, present nominal charges $z_M e$ and $-z_L e$. We designate by ε_d the energy of the d levels of a free ion, while ε_p and ε_s are corresponding energies for the valence p and s orbitals of the ligands. A good starting point is to consider the effect of the electrostatic potential due to the rest of the ions of the complex over the d levels of the cation.[50] On one hand, it raises the d levels, while, on the other, it produces a small splitting between $e_g(x^2-y^2,3z^2-r^2)$ and $t_{2g}(xy,xz,yz)$ orbitals corresponding to the so-called crystal field description. For CrX_6^{3-} complexes containing heavier X halides (X = Cl, Br, I) this contribution to $10Dq$, denoted $10Dq_{CF}$, has been shown to be negligible, while for CrF_6^{3-}, while still small, it is about six times smaller than the experimental values[59] (see section 4 for fully detailed examples). Thus, in a first approximation, $10Dq$ can be divided in two contributions, one coming from the crystal field and the second due to covalent interactions with the ligands, denoted $10Dq_{cov}$,

$$10Dq = 10Dq_{CF} + 10Dq_{cov} \quad (1)$$

To calculate this latter contribution, we consider the possibility of mixing the d orbitals of the cation with the p and s valence orbitals of the ligands. With regard to halide ligands[50]

dx.doi.org/10.1021/jp110586e |J. Phys. Chem. A 2011, 115, 1423–1432

$\varepsilon_d - \varepsilon_s \gg \varepsilon_d - \varepsilon_p$, the antibonding t_{2g} and e_g orbitals of a TM complex can be reasonably written in a first step as

$$\phi^0_{t,j} = \alpha_t \varphi^M_{t,j} - \beta_t \chi^p_{t,j} \quad (j = xy, xz, yz) \tag{2}$$

$$\phi^0_{e,j} = \alpha_e \varphi^M_{e,j} - \beta_e \chi^p_{e,j} \quad (j = 3z^2 - r^2, x^2 - y^2) \tag{3}$$

Here $\varphi^M_{t,j}$, $\varphi^M_{e,j}$ stand for pure d wave functions of the cation belonging, respectively, to t_{2g} and e_g irreducible representations (irreps) of the O_h group, while $\chi^p_{t,j}$ and $\chi^p_{e,j}$ are linear combinations of pure ligand p orbitals with the adequate symmetry.[21] For instance, the linear combination of atomic orbitals (LCAO) corresponding with the $\chi_{t,xy}$ orbital is

$$\chi^p_{t,xy} = \frac{1}{2}(\xi^p_{x,y} - \xi^p_{x,-y} + \xi^p_{y,x} - \xi^p_{y,-x}) \tag{4}$$

where $\xi^p_{i,j}$ corresponds with the p orbital oriented along the positive i-axis ($i = x, y, z$) belonging to the ligand found starting from the metal and following the direction indicated by j ($j = -x, x, -y, y, z, -z$; see Figure 1). The energies associated with the orbitals defined in eqs (2) and (3) are denoted as ε^0_t and ε^0_e, respectively. Finally, we can take into account the contribution of the s orbitals to the antibonding orbitals of the TM complex. Because there is no symmetrized linear combination of s orbitals of the ligands belonging to the t_{2g} irrep, this contribution only appears in the e_g orbital. Thus, eqs 2 and 3 can be rewritten taking into account this contribution as

$$\phi_{t,j} = \phi^0_{t,j} = \alpha_t \varphi^M_{t,j} - \beta_t \chi^p_{t,j} \quad (j = xy, xz, yz) \tag{5}$$

$$\phi_{e,j} = \alpha_e \varphi^M_{e,j} - \beta_e \chi^p_{e,j} + \gamma \chi^s_{e,j} \quad (j = 3z^2 - r^2, x^2 - y^2) \tag{6}$$

where $\chi^s_{e,j}$ is defined in a way similar to $\chi^p_{e,j}$. Since $\varepsilon_d - \varepsilon_s \gg \varepsilon_d - \varepsilon_p$, it is reasonable to assume that $\beta_e \gg \gamma$. This assumption can be verified a posteriori during numerical calculations of these parameters (see section 4). Hence, we can treat the inclusion[56] of the s orbitals into $\phi_{e,j}{}^0$ as a small perturbation to the wave function. In a simple second-order approximation we find that γ takes the value

$$\gamma = \frac{-\langle \phi^0_{e,j} | h - \varepsilon^0_e | \chi^s_{e,j} \rangle}{\varepsilon^0_e - \varepsilon_s} \tag{7}$$

and the energy correction to the e_g orbitals due to the mixing with ligand s functions is

$$\Delta\varepsilon^s_e = -\frac{|\langle \phi^0_{e,j} | h - \varepsilon^0_e | \chi^s_{e,j} \rangle|^2}{\varepsilon^0_e - \varepsilon_s} = (\varepsilon^0_e - \varepsilon_s)\gamma^2 \tag{8}$$

Therefore, the total covalent contribution to $10Dq$ can be written as

$$10Dq_{cov} = \varepsilon^0_e + \Delta\varepsilon^s_e - \varepsilon^0_t \tag{9}$$

which, in turn, can be separated in covalent p and s contributions,

$$10Dq_p = \varepsilon^0_e - \varepsilon^0_t \tag{10}$$

$$10Dq_s = \Delta\varepsilon^s_e = (\varepsilon^0_e - \varepsilon_s)\gamma^2 \tag{11}$$

With use of second-order perturbation theory, an expression similar to eq 11 can be found for $10Dq_p$,

$$10Dq_p = (\varepsilon_d - \varepsilon_p)(\beta_e{}^2 - \beta_t{}^2) \tag{12}$$

However, it must be noted that the p orbital contribution to e_g and t_{2g} orbitals is, in general, not perturbative, particularly for the heavier ligands. Thus, results obtained with eq 12 provide us only with an *estimation* of the $10Dq_p$ contribution.

$10Dq$ is not the only spectroscopic parameter to depend on covalency as it also influences the value of the interelectronic interactions. We consider, for instance, an integral such as $\langle \phi_{t,j}(r_1)\, \phi_{t,j}(r_2) | 1/r_{12} | \phi_{t,j}(r_1)\, \phi_{t,j}(r_2) \rangle$ whose value is essentially determined by the probability of finding both electrons on the metal.[60] By this argument such an integral is reduced by a factor $\alpha_t{}^4$ on passing from free Cr^{3+} to $CrX_6{}^{3-}$ complexes (X = F, Cl, Br, I). A similar reduction holds for the *B* and *C* Racah parameters widely used for describing the multiplets of TM complexes.[59]

In octahedral Cr^{3+} complexes, there are no e_g electrons in the ground state and thus β_e and γ coefficients cannot be determined through EPR measurements. However, this drawback can be circumvented by means of ab initio calculations. The strategy followed in the present work consists of deriving first the β_t, β_e, and γ coefficients which are readily accessible from ab initio calculations. Afterward, and by means of these calculated quantities at the equilibrium geometry and eq 11, we will assess the weight of $10Dq_s$ contributions along the series of $CrX_6{}^{3-}$ complexes (X = F, Cl, Br, I). Similarly, an estimation of $10Dq_p$ by means of eq 12 will be accomplished. In a further step the *R* dependence of calculated $10Dq$, β_t, β_e, and γ coefficients, and also the *B* and *C* Racah parameters, for the $CrF_6{}^{3-}$ complex will be looked into. Particular attention will be paid in this analysis to understand the origin of the different dependence displayed by $10Dq$ and the Racah parameters upon *R*.

We now focus on the total force undergone by a ligand *nucleus* (whose charge is $-z_L e$) due to the electronic density, $\rho(\mathbf{r})$, and the repulsion of other ligand nuclei and the TM nucleus. The net force on the *k* ligand of a MX_6 complex embedded in a host lattice can shortly be written as

$$F(k) = \int \rho(\mathbf{r}) \frac{\partial V_{en}}{\partial R_k}\, d\tau + \frac{\partial V_{nn}}{\partial R_k} - \frac{\partial V_{out}}{\partial R_k} \tag{13}$$

Equation 13 assumes that the electronic density, $\rho(\mathbf{r})$, is *localized* in the complex region both in the ground and in the excited state of the MX_6 complex. In that equation V_{en} and V_{nn} describe the interaction energies of the *k*-ligand nucleus with the electronic density and other nuclei of the complex, respectively. The term involving V_{out} accounts for the electrostatic interaction between all host lattice ions lying *outside* the complex and the *k*-ligand nucleus.[61] If V_{out} is not perfectly flat in the complex region, it induces a small modification on the energy levels of the complex. This quantity has been shown to be mainly responsible, among other phenomena, for the difference in color between ruby and emerald.[46,61,62]

Let $\rho_G(\mathbf{r})$ and $\rho_E(\mathbf{r}) = \rho_G(\mathbf{r}) + \Delta\rho_{GE}(\mathbf{r})$ be the electronic densities for, respectively, the ground and the excited state of the MX_6 complex *both* at the equilibrium geometry of the ground state. Obviously, in this situation $F(k) = 0$ if $\rho(\mathbf{r}) = \rho_G(\mathbf{r})$. However, if the geometry is kept but $\rho_G(\mathbf{r})$ is replaced by $\rho_E(\mathbf{r})$, this substitution leads to a net force on the *k* ligand just given by

$$F(k) = \int \Delta\rho_{GE}(\mathbf{r}) \frac{\partial V_{en}}{\partial R_k}\, d\tau \tag{14}$$

Equation 14 suggests that $F(k)$, and thus $d(10Dq)/dR$, are strongly connected to the *variations* of the electronic density in the neighborhood of the *k* nucleus which appears as a result of the

transition from the ground to the excited state.[57] A study on the behavior of $\Delta\rho_{GE}(\mathbf{r})$ for the CrF_6^{3-} unit at different R values using the results of ab initio calculations is given in section 4.5.

3. COMPUTATIONAL METHODS

We have performed first principles calculations within the framework of the density functional theory (DFT). In a first step we have carried out band structure calculations for the cubic elpasolites[55] K_2NaScF_6, Cs_2NaYCl_6, and Cs_2NaYBr_6 in order to determine the lattice parameter, a, together with the equilibrium $A^{3+}-X^-$ (A = Sc, Y; X = F, Cl, Br) distance, R_H, between the trivalent cation of the host lattice and the nearest X^- ions (Figure 1). For the sake of completeness the values of a and R_H have also been derived for the Cs_2NaScI_6 compound in a *hypothetical* elpasolite structure. These calculations were carried out using the version 5.4.4 of ABINIT code.[63] The exchange correlation energy was calculated using the Perdew−Burke−Ernzehoff (PBE) functional,[64] where the core electrons of all ions have been represented through Fritz−Haber Institute library's pseudopotentials for PBE calculations.[65] The cutoff energy for the kinetic energy of the plane wave basis set was chosen to be 40 hartrees while a k-space sampling of 8 points (2 × 2 × 2) was taken.

In a second step we have performed cluster calculations of the TM complexes using the ADF code[66] in its 2008 and 2009 versions. Here, all ions were described using the high-quality TZP basis set included in the database of the program in which each atomic orbital is described by three Slater functions plus an extra polarization one. All core electrons, including up to 1s for F, 2p for Cl, 3p for Cr, K, and Br, and 4p for I and Cs were kept frozen during the self-consistent procedure. The exchange-correlation energy was computed according to the generalized gradient approximation (GGA) using the Becke−Perdew functional.[67,68]

The geometries of $CrX_6M_8Na_6^{11+}$ (X = F, Cl, Br, I; M = K, Cs) 21 ion clusters have been optimized to obtain the local geometry around the impurity in four different cubic elpasolites, K_2NaScF_6, Cs_2NaYCl_6, Cs_2NaYBr_6, and Cs_2NaScI_6. Periodic calculations in large periodic cells, as described above, have shown that equilibrium geometries and 10Dq values, among other properties, are well-reproduced by small clusters consisting of only 21 ions due to the fact that 3d electrons are extremely localized around the impurities and its ligands.[27] In the geometry determination, only the $Cr^{3+}-X^-$ distance, R, was optimized, while the rest of the cluster ions were kept frozen at their ideal lattice position. The electrostatic potential due to the rest of the lattice ions, V_{out}, was generated by means of 155 point charges at their lattice positions with charge values previously fit to reproduce the electric field of the infinite lattice using an Evjen−Ewald scheme.[27]

In a second step, the R dependence of the n_Lp and n_Ls admixtures in the e_g orbital and the 10Dq parameter are calculated on CrX_6^{3-} (X = F, Cl, Br, I) complexes embedded in the set of point charges. This simplification can be made considering the very local character of the Cr^{3+} 3d electrons. In fact, for the antibonding e_g level the electronic density lying outside the complex in larger cluster calculations is found to be smaller than 1% for the whole set of doped elpasolites. Racah parameters B and C were calculated following the ligand field-DFT (LF-DFT) procedure[59] already employed in previous works.[27,46]

Table 1. Comparison between Calculated and Experimental Lattice Parameter Values, a, and $u = (R_H/a)$ Parameters for K_2NaScF_6, Cs_2NaYCl_6, Cs_2NaYBr_6, and Cs_2NaScI_6 Pure Lattices[a]

	a (Å)		u	
	calculated	experimental	calculated	experimental
K_2NaScF_6	8.54	8.47	0.2436	0.234
Cs_2NaYCl_6	10.47	10.48	0.2404	0.244
Cs_2NaYBr_6	11.30	11.30	0.2459	0.245
Cs_2NaScI_6	11.99		0.2413	

[a] Here R_H denotes the distance between the trivalent ion and a neighbour X^- anion (Figure 1). Experimental values have been taken from ref 55.

4. RESULTS AND DISCUSSION

4.1. Properties of CrX_6^{3-} Units in Elpasolite Hosts around the Equilibrium Geometry. The calculated values of the host lattice parameter, a, for the pure K_2NaScF_6, $Cs_2NaScCl_6$, Cs_2NaYBr_6, and Cs_2NaScI_6 lattices are collected in Table 1 together with the corresponding figures for $u = R_H/a$. R_H and a values for K_2NaScF_6, Cs_2NaYBr_6, and Cs_2NaScI_6 lattices have been derived in the present work while those corresponding to Cs_2NaYCl_6 have previously been obtained.[27] Calculated a and u values shown in Table 1 compare well with available experimental data.[55] For instance, in the case of K_2NaScF_6 the obtained a = 8.54 Å figure is only 0.8% higher than the experimental one.

A central issue in the present analysis concerns the *localization* of the three unpaired electrons coming from the Cr^{3+} impurity in the CrX_6^{3-} (X = F, Cl, Br, I) unit. Results of the present calculations on Cr^{3+}-doped K_2NaScF_6, $Cs_2NaScCl_6$, Cs_2NaYBr_6, and Cs_2NaScI_6 host lattices reveal that in the $^4A_2(t_{2g}^3)$ ground state at least 99% of the electronic charge resides in the CrX_6^{3-} octahedron, justifying the use of the complex approximation in later calculations. It is worth noting that a high degree of localization of the electronic charge has been found through electron nuclear double resonance (ENDOR) measurements carried out for the CrF_6^{3-} complex formed in $KMgF_3$ and $RbCdF_3$ perovskites.[69,70] In fact, the highest superhyperfine constant measured for F^- ligand ions is found to be about *50 times* higher than that corresponding to the second shell of fluorine ions. Moreover, a significant part of the second shell superhyperfine interaction is simply accounted for by considering the magnetic dipolar interaction of unpaired localized electrons in the CrF_6^{3-} complex with the corresponding fluorine nuclei of that shell. A similar degree of localization has been found[71] in an ENDOR study on $Mg_2AlO_4:Cr^{3+}$.

Values of the equilibrium $Cr^{3+}-F^-$ distance, R_e, obtained for the four lattices doped with Cr^{3+} through cluster calculations are displayed in Table 2. With regard to R_e = 1.95 Å derived for CrF_6^{3-} complex embedded in K_2NaScF_6 it is not unreasonable when compared to the R_e values measured for pure compounds containing CrF_6^{3-} units,[72] such as $KCrF_4$ (R_e = 1.91 Å), K_2NaCrF_6 (R_e = 1.93 Å), or Rb_2KCrF_6 (R_e = 1.94 Å). Concerning the calculated 10Dq values at R_e also shown in Table 2, it should be noticed that they reproduce the *pattern* displayed by the experimental data[36,32,59] although they are somewhat smaller. Therefore, the present calculations lead to a progressive decrease of 10Dq, calculated at the corresponding equilibrium distance, on passing from CrF_6^{3-} to CrI_6^{3-}. This trend is thus consistent with the empirical spectrochemical series.[47]

Table 2. Values of the Equilibrium $Cr^{3+}-F^-$ Distance, R_e, Calculated for CrX_6^{3-} Units in K_2NaScF_6, Cs_2NaYCl_6, Cs_2NaYBr_6, and Cs_2NaScI_6 Lattices, and Comparison between Calculated and Experimental 10*Dq* Values[a]

		10*Dq* (10^3 cm^{-1})		
X	R_e (Å)	calculated	experimental	*n*
F	1.95	14.4	15.6	4.5
Cl	2.38	11.2	12.8	4.5
Br	2.56	9.8	~12.0	4.8
I	2.92	8.9	-	5.2

[a] Available experimental data come from refs 32, 36, 59. Calculated values of the exponent *n* reflecting the dependence of 10*Dq* upon *R* around R_e are also shown.

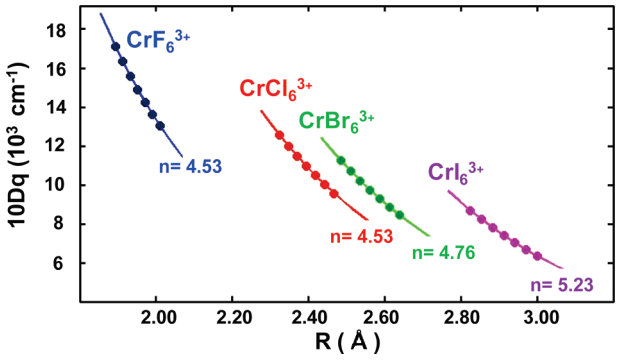

Figure 2. Variation of the 10*Dq* values with metal−ligand distance as calculated in DFT (dots). Solid lines correspond to fits carried out for calculated values using potential laws of the type KR^{-n}.

Another central point in this study concerns the *R* dependence of 10*Dq* around R_e for each one of the four CrX_6^{3-} (X = F, Cl, Br, I) complexes. Main results collected in Figure 2 point out a strong dependence of 10*Dq* upon *R* for the four CrX_6^{3-} complexes. More specifically, writing 10*Dq* in the neighborhood of the corresponding R_e metal−ligand distance

$$10Dq = KR^{-n} \quad (15)$$

it turns out that the exponent *n*, collected in Table 2, is calculated to be around 5 for all complexes. The value of the exponent *n* either measured or calculated for TM complexes with halides or oxygen as ligands is usually found[31,61] to be close to 5. This is the case, for instance, of $Al_2O_3:Cr^{3+}$, NiO, MnO, or Mn^{2+}-doped fluoroperovskites.[38−41]

4.2. Calculated Covalency Parameters for CrX_6^{3-} (X = F, Cl, Br, I) Complexes. The values of β_t^2, β_e^2, and γ^2 parameters for CrX_6^{3-} complexes calculated at R_e determined in section 4.1 are displayed in Table 3. In that table the sensitivity of such parameters to changes of the impurity−ligand distance, *R*, around R_e is also shown. In particular, we employ three exponents n_t, n_e, and n_s that are defined as

$$\beta_t^2 = C_t R^{-n_t}; \quad \beta_e^2 = C_e R^{-n_e}; \quad \gamma^2 = C_s R^{-n_s} \quad (16)$$

Values of these exponents are gathered in Table 3 for the whole series of Cr^{3+} complexes with different halides as ligands. For the sake of clarity the *R* dependence of α_t^2, β_t^2, β_e^2, and γ^2 parameters for the CrF_6^{3-} complex is also portrayed in Figure 3.

Table 3. Calculated Covalency Parameters for CrX_6^{3+} Units at the Equilibrium Distance, R_e, Derived for Complexes Embedded in K_2NaScF_6, Cs_2NaYCl_6, Cs_2NaYBr_6, and Cs_2NaScI_6 Host Lattices[a]

X	R_e (Å)	β_t^2	β_e^2	γ^2	γ^2/β_e^2	n_t	n_p	n_s
F	1.95	0.19	0.30	0.065	0.22	1.82	1.39	7.70
Cl	2.38	0.19	0.49	0.100	0.20	2.42	3.03	9.70
Br	2.56	0.18	0.51	0.081	0.16	1.87	1.74	9.42
I	2.92	0.17	0.55	0.072	0.13	0.63	3.48	10.70

[a] The values of the exponent n_t, n_p, and n_s, reflecting, respectively, the *R* dependence of β_t^2, β_e^2, and γ^2 quantities, are also shown.

As expected, the β_e^2 parameter associated with the σ covalency increases significantly on going from CrF_6^{3-} to CrI_6^{3-}. Nevertheless, β_t^2 is found to remain nearly unmodified. A similar qualitative picture emerges from the work by Brik and Ogasawara.[45] Because there are no e_g electrons in the $^4A_2(t_{2g}^3)$ ground state of Cr^{3+} complexes, only β_t^2 can be derived from experimental EPR data. From the superhyperfine tensor measured for CrF_6^{3-} in $KMgF_3$ $\beta_t^2 = 0.2$ has been obtained,[73] which compares well with the value 0.19 found for the same complex in K_2NaScF_6.

The results collected in Table 3 point out that for all CrX_6^{3-} complexes β_e^2 is certainly much higher than γ^2. Despite this fact γ^2 is found to be much more sensitive to *R* variations than β_e^2, a pattern which is always found in octahedral complexes with halides or oxygen as ligands.[46,48,49,52,53,61] In a first view, it is surprising seeing that β_e^2 is little dependent on *R* as the overlap integral $\langle\varphi_{e,j}^M|\chi_{e,j}^p\rangle$ does increase when *R* decreases. However, it has been shown that such an increase is compensated to a good extent by the significant energy increase experienced by ligand to metal charge-transfer transitions, and thus the $\varepsilon_d - \varepsilon_p$ quantity, when *R* is reduced.[50,74] A quite different situation holds however for the admixture with *deeper* n_Ls levels of halides. It was earlier pointed out[75] that the *R* dependence of γ is essentially controlled by the overlap between $\varphi_{e,j}^M$ and $\chi_{e,j}^s$ because the relative variation of the $\varepsilon_d - \varepsilon_s$ quantity is much smaller than that of $\varepsilon_d - \varepsilon_p$ as a result of the deeper character of n_Ls levels in halides and oxygen ligands.

It can be noted that the ratio $(\gamma/\beta_e)^2$ decreases along the ligand series F → Cl → Br → I. A somewhat similar situation is encountered in the series of O_h and D_{4h} complexes, where the ligand is kept but the nature of the central cation is changed.[51] In these series it has also been verified that when the total covalency increases, the ratio $(\gamma/\beta_e)^2$ lessens. Along this line it can be noticed that the calculated γ^2 value is practically unmodified on passing from CrF_6^{3-} to CrI_6^{3-}. This is in principle surprising as $\varepsilon_d - \varepsilon_s$ decreases from 23 to 10 eV on passing from CrF_6^{3-} to the more covalent CrI_6^{3-} unit. Nevertheless, according to eq 7 γ is also controlled by the $\langle\phi_{e,j}^0|\chi_{e,j}^s\rangle$ overlap, which is essentially equal to $\alpha_e\langle\varphi_{e,j}^M|\chi_{e,j}^s\rangle$. In the present calculations we have found that such a quantity is reduced from 0.107 in CrF_6^{3-} to 0.040 in CrI_6^{3-} as we move along the series. This reduction approximately compensates the decrease of $\varepsilon_d - \varepsilon_s$ on going from CrF_6^{3-} to CrI_6^{3-} and thus explains qualitatively why γ^2 is similar for both complexes, as shown in Table 3. It is important to note that the α_e parameter is found to decrease only about 7% when going from CrF_6^{3-} ($\alpha_e = 0.97$) to CrI_6^{3-} ($\alpha_e = 0.90$). Therefore, the reduction of the $\alpha_e\langle\varphi_{e,j}^M|\chi_{e,j}^s\rangle$ quantity mainly reflects that, at the corresponding equilibrium distance, the overlap between $\varphi_{e,j}^M$ and $\chi_{e,j}^s$ decreases progressively on passing from $K_2NaScF_6:Cr^{3+}$ to $Cs_2NaScI_6:Cr^{3+}$. As expected, this reduction also involves a

dx.doi.org/10.1021/jp110586e |J. Phys. Chem. A 2011, 115, 1423–1432

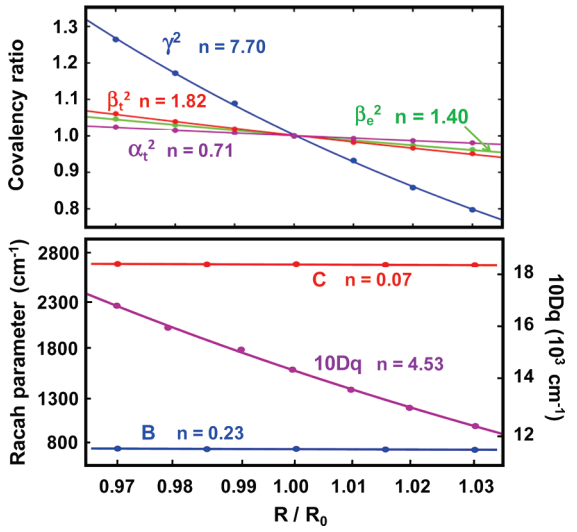

Figure 3. Relative variation with the metal−ligand distance, R, around the equilibrium in a CrF_6^{3+} complex of (a) α_t^2, β_t^2, β_e^2, and γ^2 covalency parameters and (b) $10Dq$ and the Racah parameters B and C.

higher sensitivity of γ^2 to variations of the metal−ligand distance as reflected in Table 3. In fact, while the exponent n_s is found to be equal to 7.7 for CrF_6^{3-}, the calculated value for CrI_6^{3-} is about 40% higher. It is worth noting that n_s values around 20 have been calculated for LaF_4^{2-} complexes involving the unusual La^{2+} cation.[76] This conclusion is supported by EPR data on CaF_2:La^{2+} showing that the superhyperfine lines are extremely sensitive to the application of an uniaxial stress.[76]

4.3. Contributions to $10Dq$ and the Spectrochemical Series. Seeking to gain a better insight into the spectrochemical series, we now first calculate the value of the covalent s contribution to $10Dq$, denoted $10Dq_s$, by means of eq 11 and the value of γ^2 gathered in Table 3. The obtained $10Dq_s$ values for the series of CrX_6^{3-} (X = F, Cl, Br, I) complexes at the corresponding equilibrium distances are displayed in Table 4. For the sake of completeness the p contribution, $10Dq_p$, estimated through eq 12 and β_e^2 and β_t^2 parameters from Table 3, is also given in Table 4 together with the crystal-field contribution, $10Dq_{CF}$. In that table the *approximate* quantity

$$10Dq_M = 10Dq_p + 10Dq_s + 10Dq_{CF} \qquad (17)$$

derived in the model is compared with the actual $10Dq$ figure obtained from DFT calculations for the four considered Cr^{3+} complexes.

It should be remarked that the approximate $10Dq_M$ value decreases on passing from CrF_6^{3-} to CrI_6^{3-} following the *same trend* as that displayed by the $10Dq$ values reached by means of DFT calculations. The main feature present in Table 4 is that the contribution coming from the n_Ls orbitals, $10Dq_s$, actually controls the value of $10Dq$. This is particularly important in CrF_6^{3-} (embedded in K_2NaScF_6), where it accounts for 86% the total $10Dq$ value, but even in CrI_6^{3-} (embedded in Cs_2NaScI_6) its contribution accounts for 70% of the total $10Dq$ value. All these ab initio results thus support previous semiempirical calculations on CrF_6^{3-} complexes, pointing out that the $10Dq$ value is clearly dominated by the $10Dq_s$ contribution.[54] According to eq 11 $10Dq_s$ depends on both γ^2 and $\varepsilon_d - \varepsilon_s$ quantities. Since γ^2 is found to be the same for CrF_6^{3-} and CrI_6^{3-} units (Table 3), while $\varepsilon_d - \varepsilon_s$ decreases on passing from the former to the latter complex, this leads to a reduction of the dominant contribution to $10Dq$. Because, according to Table 4, the quantity $10Dq - 10Dq_s \ll 10Dq$, this fact explains the progressive decrease of $10Dq$ on passing from CrF_6^{3-} to CrI_6^{3-} reflected in the spectrochemical series.[47]

Table 4. Values of $10Dq$ Parameter Obtained by Means of DFT Calculations Performed at the Equilibrium R_e Distance for the Four CrX_6^{3+} Units Embedded in the Elpasolite Lattices[a]

X	$10Dq$	$10Dq_s$	$10Dq_p$	$10Dq_{CF}$	$10Dq_M$
F	14.4	12.4	3.8	1.6	17.8
Cl	11.2	11.7	4.8	0.5	17.0
Br	9.8	8.9	3.8	0.3	12.9
I	8.9	6.2	2.3	0.1	8.6

[a] Values of crystal-field contribution, $10Dq_{CF}$, and covalent contributions, $10Dq_s$ (calculated by means of eq 11) and $10Dq_p$ (estimated by means of eq 12), are also shown, together with the sum of the three contributions, $10Dq_M$. All values are given in 10^3 cm^{-1} units.

4.4. Different Sensitivity of $10Dq$ and Racah Parameters to the Metal−Ligand Distance. The present analysis also sheds light on the main cause behind the significant R dependence of $10Dq$ corresponding to *a given* complex. Indeed if, according to Figure 3a and Table 3, γ^2 strongly depends upon R while β_e^2 varies only slightly when R is modified, one can expect an important sensitivity of $10Dq$ to R changes because $10Dq_s$ is the dominant contribution when compared to $10Dq_p$. Moreover, this simple reasoning also tells us that the exponent n involved in eq 15 should be smaller than n_s, describing in eq 16 the R dependence of γ^2. It is worth noting now that in complexes such as MnF_6^{4-}, NiF_6^{4-}, or FeF_6^{4-}, where there are unpaired e_g electrons in the ground state, the condition $n_s > n$ has been verified experimentally by means of EPR and ENDOR techniques on complexes placed in different host lattices.[49,53,61,75]

On the contrary, calculated values for the Racah parameters are much less sensitive to metal−ligand distance variations. LF-DFT calculations on *free* Cr^{3+} led to the values of B_0 = 1013 cm^{-1} and C_0 = 3688 cm^{-1}. When the cation gives rise to a CrF_6^{3-} complex embedded in K_2NaScF_6, LF-DFT calculations yield the values B = 772 cm^{-1} and C = 2630 cm^{-1}. These results are in reasonable agreement with previously reported values for Cr^{3+} impurities in fluorides.[77]

Concerning the calculated R dependence of the two B and C Racah parameters we take as a guide the case of the CrF_6^{3-} complex whose results are portrayed in Figure 3b. It can be noticed that, at variance with what is found for $10Dq$, the calculated Racah parameters are found to be almost independent of R. This result is consistent with other theoretical calculations on TM complexes and available experimental data.[39,40,43,46] The Racah parameters are essentially dependent upon the probability of finding the two active electrons on the central cation of the complex.[60] For this reason they depend basically on quantities such as α_t^4 which reflect the *global* covalency. As shown in Figure 3a, α_t^2 is not significantly dependent on R, which is thus behind the behavior of B and C Racah parameters portrayed in Figure 3b.

The present analysis thus sheds light on the microscopic origin of the quite different R dependence shown by $10Dq$ and the Racah parameters. Indeed the $10Dq$ parameter is found to arise mostly from the *small* n_Ls admixture in the antibonding $e_g(\sim x^2-y^2, 3z^2-r^2)$ level reflected in the γ^2 quantity. By contrast,

this n_Ls admixture is practically unimportant with regard to two-center integrals such as $\langle \phi_{t,j}(r_1)\, \phi_{t,j}(r_2)|1/r_{12}|\phi_{t,j}(r_1)\, \phi_{t,j}(r_2)\rangle$ and Racah parameters depending on the global covalency.

The existence of distinct mechanisms behind the R dependence of $10Dq$ and Racah parameters allows one to understand *microscopically* well-known experimental features. For instance, the separation between the first excited states $^4T_2$ and ^2E for d^3 impurities depends on the ratio $10Dq/B$ according to the Tanabe−Sugano diagrams.[21] As the emission in these systems arise from the first excited state, applying pressure on systems such as $K_2NaScF_6:Cr^{3+}$, $KMgF_3:Cr^{3+}$, or $LiCaAlF_6:Cr^{3+}$ allows one to tune either a broad band emission (from $^4T_2$) or a sharp one.[24,25,78] The present analysis clearly reveals that this tuning is possible thanks to the *different response* to pressure of $10Dq$ and B parameters which also has another relevant consequence. In fact, if the energy of an excited state with respect to the ground one is called E, the bandwidth, the Huang−Rhys factor of the symmetric mode, and the Stokes shift all depend[26,27,31,35,79] on dE/dR. By virtue of this fact, since the energy of the ^2E state only depends on the B parameter,[21] this gives rise to a sharp line (bandwidth in the range of 1−10 cm^{-1}) with zero Stokes shift.[80] By contrast, since $E = 10Dq$ for the $^4T_2$ state, the emission from this state gives rise[32−34,36,73,77,78] to a broad band (bandwidth around 2000 cm^{-1}) and Stokes shift in the range of 2000−3000 cm^{-1}.

4.5. Analysis of the Differential Electronic Density, $\Delta\rho_{GE}$. The analysis carried out in the preceding section strongly supports that the small n_Ls admixture involved in the antibonding e_g orbital plays a key role for understanding the values of $10Dq$ and the exponent n. Because the differential electronic density, $\Delta\rho_{GE}$, is related to $d(10Dq)/dR$ and thus to the force, $F(k)$, exerted on the k-ligand nucleus on passing from the $^4A_2(t_{2g}^3)$ ground state to the excited $t_{2g}^2e_g$ configuration, we are now going to visualize the form of $\Delta\rho_{GE}$ at different R values around R_e. As it has already been pointed out,[35,57] the first excited state $^4T_{2g}(t_{2g}^2e_g)$ is not an orbital singlet. For this reason after the $^4A_{2g}(t_{2g}^3) \rightarrow {}^4T_{2g}(t_{2g}^2e_g)$ excitation an anisotropic Jahn−Teller force appears in addition to an isotropic force along the breathing mode. Therefore, if we want to see *only* the isotropic component of the force, we can use the isotropic part of the electron density corresponding to the $(3z^2-r^2)^{0.5}(x^2-y^2)^{0.5}(xy)^{2/3}(xz)^{2/3}(yz)^{2/3}$ electronic configuration with fractional occupation.[57] The change of electronic density, $\Delta\rho_{GE}(\mathbf{r})$, on passing from the ground state ($(xy)^1(xz)^1(yz)^1$ configuration) to such an excited state is just given by[57]

$$\Delta\rho_{GE}(\mathbf{r}) = (1/2)[\rho_{3z^2-r^2}(\mathbf{r}) + \rho_{x^2-y^2}(\mathbf{r})] - (1/3)[\rho_{xy}(\mathbf{r}) + \rho_{xz}(\mathbf{r}) + \rho_{yz}(\mathbf{r})] \quad (18)$$

$$\rho_i(\mathbf{r}) = |\phi_i|^2 \quad (i = e, 3z^2-r^2; e, x^2-y^2; t, xy; t, xz; t, yz)$$

where one-electron ϕ_i wave functions were defined in eqs 5 and 6. Bearing in mind that ϕ_{e,x^2-y^2} and $\phi_{e,3z^2-r^2}$ transform like $\sqrt{3}(x^2-y^2)$ and $(3z^2-r^2)$, respectively, and that $\phi_{xy} \sim xy$, it can easily be verified that $\Delta\rho_{GE}(\mathbf{r})$ exhibits cubic symmetry, thus leading to the same force on all ligands.

The form of $\Delta\rho_{GE}(\mathbf{r})$, derived from the present ab initio calculations, at two R values for the CrF_6^{3-} complex, is portrayed in Figure 4. We now have a look on the behavior of $\Delta\rho_{GE}(\mathbf{r})$ around a given ligand nucleus. It can be noticed that the electronic density $\Delta\rho_{GE}(\mathbf{r})$ in the outside part of the complex

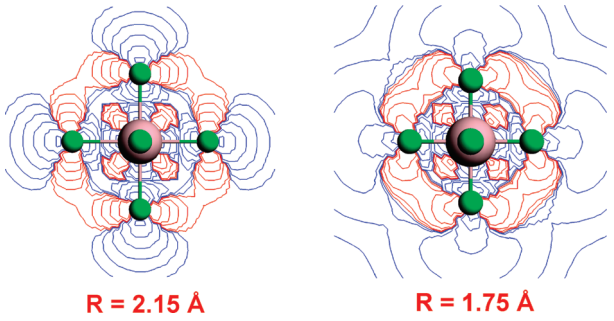

Figure 4. Equidensity contours of the difference density function, $\Delta\rho_{GE}$, for a CrF_6^{3+} complex when the metal−ligand distance, R, is 2.15 (left) and 1.75 Å (right). Blue (red) contour lines correspond to regions with $\Delta\rho_{GE} > 0$ ($\Delta\rho_{GE} < 0$).

just behind a given nucleus grows significantly when R is progressively reduced. Moreover, comparing the form of $\Delta\rho_{GE}(\mathbf{r})$ in that region for R = 2.15 Å and R = 1.75 Å, one can easily notice the increase of the 2s(F) admixture into the e_g wave function in the latter case. In fact, the *lobes* of electronic accumulation ($\Delta\rho_{GE} > 0$) associated with two adjacent ligands are well-separated when R = 2.15 Å, while they intersect when the Cr^{3+}−F^- distance becomes smaller. It should be pointed out now that this electronic density displaced toward the external region of the complex as a result of a $t_{2g} \rightarrow e_g$ excitation appears as a fundamental contribution to the isotropic *outward* force on any ligand.

It is worth noting here that an outward force on a ligand requires that the electronic density $\Delta\rho_{GE}$ around a ligand nucleus is, in general, higher in the external region of the complex ($|r| > R$) than in the region lying between metal and ligand nuclei where $|r| < R$. This imbalance is greatly helped by the strong antibonding character of the e_g wave function. We consider, for example, the upper ligand in Figure 1. In view of eqs 5, 6, and 18, the contribution to $\Delta\rho_{GE}(\mathbf{r})$ around the ligand in the positive z direction (see Figure 1) coming from σ bonding, shortly called $\delta(\sigma)$, can be written as

$$\delta(\sigma) \approx \frac{1}{6}[(-\beta_e\xi^p_{z,z} + \gamma\xi^s_z)^2 + 2\sqrt{3}\alpha_e\varphi^M_{e,3z^2-r^2}(-\beta_e\xi^p_{z,z} + \gamma\xi^s_z)] \quad (19)$$

In eq 19 the first and second terms describe the so-called ligand−ligand and metal−ligand contributions, respectively. As the hybrid contribution from a ligand orbital with σ character, $-\beta_e\xi^p_{z,z} + \gamma\xi^s_z$, reinforces the electronic density in the middle region between the ligand and the central cation, the ligand−ligand contribution *alone* would give rise to an *inward* ligand relaxation, a point not well clarified in a previous work.[57] This situation is however significantly modified thanks to the metal−ligand contribution in eq 19, which reduces the electronic density in the middle region since the orbital is *antibonding*, thus making possible a net outward force on a ligand.

5. FINAL REMARKS

The present ab initio calculations reproduce the different dependence on the metal−ligand distance of $10Dq$ and Racah parameters observed experimentally. At the same time they reproduce the progressive decrease of $10Dq$ on passing from CrF_6^{3-} to CrI_6^{3-} reflected in the spectrochemical series. Moreover, the

analysis carried out in this work using the approximate expression 17 and the results of ab initio calculations strongly support that the 10*Dq* splitting parameter comes mostly from the small admixture of deep n_Ls ligand orbitals in the antibonding $e_g(\sim x^2-y^2,3z^2-r^2)$ orbital. Therefore, this unexpected conclusion provides us with a link between 10*Dq* and the isotropic superhyperfine constant, A_s, which can be measured when there are unpaired electrons occupying the $e_g(\sim x^2-y^2,3z^2-r^2)$ level[73] of octahedral complexes. Taking into account that A_s is a direct reflection of γ^2, it was early recognized that A_s is strongly dependent on the impurity−ligand distance and thus can be used for getting reliable information on *R* from EPR and ENDOR measurements.[75,46,49,53] The present results point out that the sensitivity of 10*Dq* to *R* variations is also related to the strong dependence of γ^2 on *R*. Similarly, the recent findings of ferroelectricity in highly compressed $BaTiO_3$ and $PbTiO_3$ materials have been associated with the increased covalency of e_g orbitals of Ti with the 2s orbitals of the oxygen ions inside the TiO_6^{4-} complexes, revealing how these deep and apparently inactive orbitals can trigger very strong structural effects.[81]

At variance with what happens for the n_Lp admixture in $e_g(\sim x^2-y^2,3z^2-r^2)$ the present results show that the n_Ls admixture is practically unmodified when comparing CrF_6^{3-} and CrI_6^{3-} units. Because the dominant contribution to 10*Dq* depends on $(\varepsilon_e^0 - \varepsilon_s)\gamma^2$ the reduction of $\varepsilon_e^0 - \varepsilon_s$ on passing from CrF_6^{3-} to CrI_6^{3-} allows one to understand the trend reflected in the spectrochemical series.[47]

In summary, in this work we show that ab initio calculations are useful not only for predicting the value of 10*Dq* but especially for understanding the subtle origin of a number of phenomena. In particular, our results can be used to explain the very different dependence of 10*Dq* and the Racah parameters with the metal−ligand distance. Further work along this line is now underway.

AUTHOR INFORMATION

Corresponding Author

*E-mail: aramburj@unican.es.

ACKNOWLEDGMENT

The support by the Spanish Ministerio de Ciencia y Tecnología under Project FIS2009-07083 is acknowledged.

REFERENCES

(1) Gatteschi, D.; Sessoli, R. Quantum Tunneling of Magnetization and Related Phenomena in Molecular Materials. *Angew. Chem., Int. Ed.* **2003**, *42*, 268–297.

(2) Friedman, J. R.; Sarachik, M. P.; Tejada, J.; Ziolo, R. Macroscopic Measurement of Resonant Magnetization Tunneling in High-Spin Molecules. *Phys. Rev. Lett.* **1996**, *76*, 3830–3833.

(3) Cirera, J.; Ruiz, E.; Alvarez, S.; Neese, F.; Kortus, J. How to Build Molecules with Large Magnetic Anisotropy. *Chem.—Eur. J.* **2009**, *15*, 4078–4087.

(4) García-Fernández, P.; Senn, F.; Daul, C. A.; Aramburu, J. A.; Barriuso, M. T.; Moreno, M. The Giant Magnetic Anisotropy Energy of Fe^+ Ions in $SrCl_2$. *Phys. Chem. Chem. Phys.* **2009**, *11*, 7545–7548.

(5) Siegbahn, P. E. M.; Blomberg, M. R. A. Transition Metal Systems in Biochemistry Studied by High Accuracy Quantum Chemical Methods. *Chem. Rev.* **2000**, *100*, 421–437.

(6) Kumar, S.; Dhar, D. N.; Saxena, P. N. Applications of Metal Complexes of Schiff Bases. *J. Sci. Ind. Res.* **2009**, *68*, 181–187.

(7) Albrecht, T.; Guckian, A.; Ulstrup, J.; Vos, J. G. Transistor-like Behavior of Transition Metal Complexes. *Nano Letters* **2005**, *5*, 1451–1455.

(8) Jansen, M.; Letschert, H. P. Inorganic Yellow-Red Pigments without Toxic Metals. *Nature* **2000**, *404*, 980–982.

(9) Nassau, K. *Color for Science, Art and Technology*; Elsevier: Amsterdam, 1998.

(10) Reinen, D.; Atanasov, M.; Lee, S. L. Second-Sphere Ligand Field Effects on Oxygen Ligator Atoms and Experimental Evidence—The Transition Metal−Oxygen Bond in Oxidic Solids. *Coord. Chem. Rev.* **1998**, *175*, 91–158.

(11) Holder, E.; Langeveld, B. M. W.; Schubert, U. S. New Trends in the Use of Transition Metal−Ligand Complexes for Applications in Electroluminescent Devices. *Adv. Mater.* **2005**, *17*, 1109–1121.

(12) Burns, R. G. *Mineralogical Applications of Crystal Field Theory*; Cambridge University Press: Cambridge, U.K., 1993.

(13) Juhin, A.; Calas, G.; Cabaret, D.; Galoisy, L.; Hazemann, J. L. Structural Relaxation around Substitutional Cr^{3+} in $MgAl_2O_4$. *Phys. Rev. B* **2007**, *76*, No. 054105.

(14) Halenius, U.; Andreozzi, G. B.; Skogby, H. Structural Relaxation around Cr^{3+} and the Red-Green Color Change in the Spinel (Sensu Stricto)-magnesiochromite ($MgAl_2O_4$−$MgCr_2O_4$) and Gahnite-Zincochromite ($ZnAl_2O_4$-$ZnCr_2O_4$) Solid-Solution Series. *Am. Mineral.* **2010**, *95*, 456–462.

(15) Jahren, A. H.; Kruger, M. B.; Jeanloz, R. J. Alexandrite as a High-Temperature Pressure Calibrant, and Implications for the Ruby-Fluorescence Scale. *J. Appl. Phys.* **1992**, *71*, 1579–1582.

(16) Syassen, K. Ruby under Pressure. *High Pressure Res.* **2008**, *28*, 75–126.

(17) Powell, R. C. *Physics of Solid-State Laser Materials*; Springer-Verlag: New York, 1998.

(18) Samtleben, T. A.; Hulliger, J. $LiCaAlF_6$ and $LiSrAlF_6$: Tunable Solid-State Laser Host Materials. *Opt. Lasers Eng.* **2005**, *43*, 251–262.

(19) Kornev, I. A.; Bellaiche, L. The Nature of Ferroelectricity under Pressure. *Phase Transit.* **2007**, *80*, 385–413.

(20) Garcia-Fernandez, P.; Trueba, A.; Garcia-Lastra, J. M.; Barriuso, M. T.; Moreno, M.; Aramburu, J. A. In *The Jahn-Teller Effect. Fundamentals and Implications for Physics and Chemistry*; Koeppel, H., Barentzen, H., Yarkony, D. R., Eds.; Springer-Verlang: Berlin, Germany, 2009.

(21) Sugano, S.; Tanabe, Y.; Kamimura, H. *Multiplets of Transition-Metal Ions in Crystals*; Academic Press: New York, 1970.

(22) Xu, W. M.; Naaman, O.; Rozenberg, G. Kh.; Pasternak, M. P.; Taylor, R. D. Pressure-Induced Breakdown of a Correlated System: The Progressive Collapse of the Mott-Hubbard State in $RFeO_3$. *Phys. Rev. B* **2001**, *64*, No. 094411.

(23) Xu, W. M.; Rozenberg, G. Kh.; Pasternak, M. P.; Kertzer, M.; Kurnosov, A.; Dubrovinsky, L. S.; Pascarelli, S.; Muñoz, M.; Vaccari, M.; Hanfland, M.; Jeanloz, R. Pressure-Induced Fe↔Cu Cationic Valence Exchange and Its Structural Consequences: High-Pressure Studies of Delafossite $CuFeO_2$. *Phys. Rev. B* **2010**, *81*, No. 104110.

(24) Dolan, J. F.; Kappers, L. A.; Bartram, R. H. Pressure and Temperature Dependence of Chromium Photoluminescence in K_2NaGaF_6:Cr^{3+}. *Phys. Rev. B* **1986**, *33*, 7339–7340.

(25) Sanz-Ortiz, M. N.; Rodriguez, F.; Hernández, I.; Valiente, R.; Kück, S. Origin of the ^2E↔$^4T_2$ Fano Resonance in Cr^{3+}-Doped $LiCaAlF_6$: Pressure-Induced Excited-State Crossover. *Phys. Rev. B* **2010**, *81*, No. 045114.

(26) Seijo, L.; Barandiaran, Z. High Pressure Effects on the Structure and Spectroscopy of V^{3+} Substitutional Defects in Cs_2NaYCl_6. An ab Initio Embedded Cluster Study. *J. Chem. Phys.* **2003**, *118*, 1921–1928.

(27) García-Lastra, J. M.; Moreno, M.; Barriuso, M. T. Pressure Effects on $CrCl_6^{3-}$ Embedded in Cubic Cs_2NaMCl_6 (M = Sc,Y) Lattices: Study through Periodic and Cluster Calculations. *J. Chem. Phys.* **2008**, *128*, 144708–144718.

(28) Pollini, I.; Spinolo, G.; Benedek, G. Vibrational Structure of Crystal-Field Spectra in Layered 3*d*-Metal Dihalides. *Phys. Rev. B* **1980**, *22*, 6369–6390.

(29) Rodriguez, F.; Breñosa, A. G.; Aramburu, J. A.; Moreno, M.; Calleja, J. M. Optical and Raman Investigation of $NH_4Cl:Cu^{2+}$. *J. Phys. C* **1987**, *20*, L641–L648.

(30) McDonald, R. G.; Hitchman, M. A. Electronic "d−d" Spectra of the Planar Tetrachlorocuprate(2−) Ions in Bis(methadonium) Tetrachlorocuprate(II) and Bis(creatininium) Tetrachlorocuprate(II): Analysis of the Temperature Dependence and Vibrational Fine Structure. *Inorg. Chem.* **1986**, *25*, 3273–3281.

(31) Moreno, M.; Barriuso, M. T.; Aramburu, J. A. The Huang-Rhys Factor $S(a_{1g})$ for Transition-Metal Impurities: A Microscopic Insight. *J. Phys.: Condens. Matter* **1992**, *4*, 9481–9488.

(32) Knochenmuss, R.; Reber, C.; Rajasekharan, M. V.; Gudel, H. U. Broadband Near-Infrared Luminescence of Cr^{+3} in the Elpasolite Lattices $Cs_2NaInCl_6$, Cs_2NaYCl_6, and Cs_2NaYBr_6. *J. Chem. Phys.* **1986**, *85*, 4280–4289.

(33) Marco de Lucas, M. C.; Rodriguez, F.; Dance, J. M.; Moreno, M.; Tressaud, A. Luminescence of the New Elpasolite Rb_2KGaF_6 Doped with Cr^{3+}. *J. Lumin.* **1991**, *48*−*9*, 553–557.

(34) Dolan, J. F.; Rinzler, A. G.; Kappers, L. A.; Bartram, R. H. Pressure and Temperature Dependence of Chromium Photoluminescence Spectra in Fluoride Elpasolites. *J. Phys. Chem. Solids* **1992**, *53*, 905–912.

(35) Barriuso, M. T.; Aramburu, J. A.; Moreno, M. Coupling with the Jahn-Teller Mode for Triplet States of MF_6 (M = Mn^{2+}, Cr^{3+}) Complexes: Dependence on the M-F Distance and Influence on the Stokes Shift. *Phys. Status Solidi B* **1996**, *196*, 193–208.

(36) Wenger, O. S.; Gudel, H. U. Optical Spectroscopy of $CrCl_6^{3-}$ Doped $Cs_2NaScCl_6$: Broadband Near-Infrared Luminescence and Jahn-Teller Effect. *J. Chem. Phys.* **2001**, *114*, 5832–5841.

(37) Wissing, K.; Aramburu, J. A.; Barriuso, M. T.; Moreno, M. Optical Properties due to Cr^{4+} in Oxides: Density Functional Study. *Solid State Commun.* **1998**, *108*, 1001–1005.

(38) Drickamer, H. G. Effect of Interionic Distance on the Ligand Field in NiO. *J. Chem. Phys.* **1967**, *47*, 1880.

(39) Rodriguez, F.; Moreno, M. Dependence of the Optical Spectrum of MnF_6^{4-} on the Mn^{2+}−F^- Distance. *J. Chem. Phys.* **1986**, *84*, 692–697.

(40) Duclos, S.; Vohra, Y. K.; Ruoff, A. L. Pressure Dependence of the $^4T_2$ and $^4T_1$ Absorption Bands of Ruby to 35 GPa. *Phys. Rev. B* **1990**, *41*, 5372–5381.

(41) Mita, Y.; Sakai, Y.; Izaki, D.; Kobayashi, M.; Endo, S.; Mochizuki, S. Optical Study of MnO under High Pressure. *Phys. Status Solidi B* **2001**, *223*, 247–251.

(42) Garcia-Fernandez, P.; Aramburu, J. A.; Barriuso, M. T.; Moreno, M. Key Role of Covalent Bonding in Octahedral Tilting in Perovskites. *J. Phys. Chem. Lett.* **2010**, *1*, 647–651.

(43) Luaña, V.; Bermejo, M.; Flórez, M.; Recio, J. M.; Pueyo, L. Effects of a Quantum-Mechanical Lattice on the Electronic Structure and *d*−*d* Spectrum of the $(MnF_6)^{4-}$ Cluster in Mn^{2+}:$KZnF_3$. *J. Chem. Phys.* **1989**, *90*, 6409–6421.

(44) López-Moraza, S.; Pascual, J. L.; Barandiarán, Z. *Ab initio* Model Potential Embedded-Cluster Study of V^{2+}-Doped Fluoroperovskites: Effects of Different Hosts on the Local Distortion and Electronic Structure of $^4T_{2g}$−$^4A_{2g}$ Laser Levels. *J. Chem. Phys.* **1995**, *103*, 2117–2125.

(45) Brik, M. G.; Ogasawara, K. Microscopic Analysis of the Crystal Field Strength and Lowest Charge Transfer Energies in the Elpasolite Crystals Cs_2NaYX_6 (X = F, Cl, Br) Doped with Cr^{3+}. *Phys. Rev. B* **2006**, *74*, No. 045105.

(46) Trueba, A.; Garcia-Lastra, J. M.; Barriuso, M. T.; Aramburu, J. A.; Moreno, M. Influence of Internal Electric Fields on Bonding and Properties of Impurities in Insulators: Mn^{2+} in $LiBaF_3$ and Normal Perovskites. *Phys. Rev. B* **2008**, *78*, 075108.

(47) Jörgensen, C. K. *Modern Aspects of Ligand Field Theory*; North Holland: Amsterdam, 1971.

(48) Emery, J.; Leble, A.; Fayet, J. C. Superhyperfine Interactions and Covalency Contribution to Axial Zero Field Splitting for $|MnF_6|^{4-}$ Complexes in Fluorides. *J. Phys. Chem. Solids* **1981**, *9*, 789–798.

(49) Aramburu, J. A.; Paredes, J. I.; Barriuso, M. T.; Moreno, M. Local Relaxation around Fe^{3+} in Fluorides: Influence on Electronic Properties. *Phys. Rev. B* **2000**, *61*, No. 6525.

(50) Moreno, M.; Aramburu, J. A.; Barriuso, M. T. Electronic Properties and Bonding in Transition Metal Complexes: Influence of Pressure. *Struct. Bonding (Berlin)* **2004**, *106*, 127–152.

(51) Moreno, M. The Degree of Hybridization in Paramagnetic Complexes. *Solid State Commun.* **1981**, *38*, 1045–1048.

(52) Rousseau, J. J.; Leble, A.; Fayet, J. C. Examen des paramètres de l'Hamiltonien de spin de Mn^{2+} substitué a M, dans les fluoperovskites AMF_3, dans la phase tétragonale de $RbCaF_3$ et dans les composés A_2MF_4. *J. Phys. (Paris)* **1978**, *39*, 1215–1224.

(53) Villacampa, B.; Cases, R.; Orera, V. M.; Alcalá, R. EPR and Optical Study of Ni^{2+} Ions in $CsCaF_3$ and $CsCdF_3$. *J. Phys. Chem. Solids* **1994**, *55*, 263–272.

(54) Moreno, M.; Aramburu, J. A.; Barriuso, M. T. Coupling Constants with Vibrations and the 10*Dq* Parameter for Cr^{3+} in Fluorides: Microscopic Analysis. *Phys. Rev. B* **1997**, *56*, 14423–14427.

(55) Reber, C.; Gudel, H. U.; Meyer, G.; Schleid, T.; Daul, C. A. Optical Spectroscopic and Structural Properties of Vanadium(3+)-Doped Fluoride, Chloride, and Bromide Elpasolite Lattices. *Inorg. Chem.* **1989**, *28*, 3249–3258.

(56) McWeeny, R.; Sutcliffe, B. T. *Methods of Molecular Quantum Mechanics*; Academic Press: London, 1976.

(57) Garcia-Fernandez, P.; Garcia-Lastra, J. M.; Aramburu, J. A.; Barriuso, M. T.; Moreno, M. Strong Dependence of 10Dq on the Metal−Ligand Distance: Key Role Played by the s−p Hybridization on Ligands. *Chem. Phys. Lett.* **2006**, *426*, 91–95.

(58) Anderson, P. W. Theory of Magnetic Exchange Interactions: Exchange in Insulators and Semiconductors. *Solid State Phys.* **1963**, *14*, 99–214.

(59) Atanasov, M.; Daul, C. A.; Rauzy, C. New Insights into the Effects of Covalency on the Ligand Field Parameters: A DFT Study. *Chem. Phys. Lett.* **2003**, *367*, 737–746.

(60) Curie, D.; Barthou, C.; Canny, B. Covalent Bonding of Mn^{2+} Ions in Octahedral and Tetrahedral Coordination. *J. Chem. Phys.* **1974**, *61*, 3048–3062.

(61) Moreno, M.; Barriuso, M. T.; Aramburu, J. A.; Garcia-Fernandez, P.; Garcia-Lastra, J. M. Microscopic Insight into Properties and Electronic Instabilities of Impurities in Cubic and Lower Symmetry Insulators: The Influence of Pressure. *J. Phys.: Condens. Matter* **2006**, *18*, R315–R360.

(62) Garcia-Lastra, J. M.; Barriuso, M. T.; Aramburu, J. A.; Moreno, M. Origin of the Different Color of Ruby and Emerald. *Phys. Rev. B* **2005**, *72*, No. 113104.

(63) Gonze, X.; Rignanese, G. M.; Verstraete, M.; et al. A Brief Introduction to the ABINIT Software Package. *Z. Kristallogr.* **2005**, *220*, 558–562.

(64) Perdew, J. P.; Burke, K.; Ernzerhof, M. Generalized Gradient Approximation Made Simple. *Phys. Rev. Lett.* **1996**, *77*, 3865–3868.

(65) Fuchs, M.; Scheffler, M. Ab Initio Pseudopotentials for Electronic Structure Calculations of Poly-atomic Systems Using Density-Functional Theory. *Comput. Phys. Commun.* **1999**, *119*, 67–98.

(66) te Velde, G.; Bickelhaupt, F. M.; Baerends, E. J.; Guerra, C. F.; van Gisbergen, S. J. A.; Snijders, J. G.; Ziegler, T. Chemistry with ADF. *J. Comput. Chem.* **2001**, *22*, 931–967.

(67) Becke, A. D. Density-Functional Exchange-Energy Approximation with Correct Asymptotic Behavior. *Phys. Rev. A* **1988**, *38*, 3098–3100.

(68) Perdew, J. P. Density-Functional Approximation for the Correlation Energy of the Inhomogeneous Electron Gas. *Phys. Rev. B* **1986**, *33*, 8822–8824.

(69) Davies, J. J.; Horai, K. The Hyperfine Interactions of Fluorine Ions in the Vicinity of Cr^{3+} and Cr^+ in $KMgF_3$. II. Overlap Contributions to the Second Nearest Fluorine Interaction. *J. Phys. C* **1971**, *4*, 682–688.

(70) Studzinski, P.; Spaeth, J.-M. ENDOR Investigation of Cr^{3+} Centres in the Tetragonal Phase of $RbCdF_3$. *Phys. Status Solidi B* **1986**, *136*, 735–742.

(71) Bravo, D.; Bottcher, R. Electron-Nuclear Double-Resonance Investigations on Cr^{3+} Ions in Natural $MgAl_2O_4$ Spinel. *J. Phys.: Condens. Matter* **1992**, *4*, 7295–7306.

(72) Luaña, V.; Fernández Rodrigo, G.; Francisco, E.; Pueyo, L. Core Projection Effects in Near-ab-Initio Valence Calculations: II. Ground State Geometry of Octahedral Chromium (I, II, III, and IV) Hexafluorides. *J. Solid State Chem.* **1987**, *66*, 263–282.

(73) Owen, J.; Thornley, J. H. M. Covalent Bonding and Magnetic Properties of Transition Metal Ions. *Rep. Prog. Phys.* **1966**, *29*, 675–728.

(74) Aramburu, J. A.; Moreno, M.; Barriuso, M. T. How Do the Electronic Properties of d^9 Impurities Depend on Metal-Ligand Distances? Application to Ni^+, Cu^{2+} and Ag^{2+} Systems. *J. Phys.: Condens. Matter* **1992**, *4*, 9089–9112.

(75) Barriuso, M. T.; Moreno, M. Determination of the Mn^{2+}-F^- Distance from the Isotropic Superhyperfine Constant for $[MnF_6]^{4-}$ in Ionic Lattices. *Phys. Rev. B* **1984**, *29*, 3623–3631; Determination of the Ni^+-F^- Distance for Square-Planar and Linear Centers in LiF:Ni^+ and NaF:Ni^+. *Solid State Commun.* **1984**, *51*, 335–338.

(76) García-Lastra, J. M.; Bill, H.; Barriuso, M. T.; Aramburu, J. A.; Moreno, M. Anomalous Superhyperfine Tensor Observed in BaFCl Doped with the $5d^1$ Ion La^{2+}: Role of 5d-4f Hybridization. *Phys. Rev. B* **2007**, *75*, No. 155118.

(77) Hernández, I.; Rodriguez, F.; Tressaud, A. Optical Properties of the $(CrF_6)^{3-}$ Complex in A_2BMF_6:Cr^{3+} Elpasolite Crystals: Variation with M−F Bond Distance and Hydrostatic Pressure. *Inorg. Chem.* **2008**, *47*, 10288–10298.

(78) Mortier, M.; Wang, Q.; Buzare, J. Y.; Rousseau, M.; Piriou, B. Optical Studies of Cr^{3+} in $KMgF_3$: Time-Resolved Site-Selective Spectroscopy and Experimental Evidence of Spin-Orbit Coupling. *Phys. Rev. B* **1997**, *56*, 3022–3031.

(79) Bourgoin, J.; Lanoo, M. *Point Defects in Semiconductors II*; Springer-Verlag: Berlin, 1983.

(80) Jacobsen, S. M.; Tissue, B. M.; Yen, W. M. New Methods for Studying the Optical Properties of Metal Ions in Solids. *J. Phys. Chem.* **1992**, *96*, 1547–1553.

(81) Kornev, I. A.; Bellaiche, L.; Bouvier, P.; Janolin, P.-E.; Dkhil, B.; Kreisel, J. Ferroelectricity of Perovskites under Pressure. *Phys. Rev. Lett.* **2005**, *95*, 196804.

(82) Woods, A. M.; Sinkovits, R. S.; Charpie, J. C.; Huang, W. L.; Bartram, R. H.; Rossi, A. R. Computer Modeling of the Optical Properties of Substitutional Chromium Impurities in Halide Elpasolites. *J. Phys. Chem. Solids* **1993**, *54*, 543–552.

■ NOTE ADDED AFTER ASAP PUBLICATION

This article posted ASAP on February 4, 2011. Equation 7 has been revised. The correct version posted on February 9, 2011.